

# An IGDT-Based Energy Management System for Local Energy Communities Considering Phase-Change Thermal Energy Storage

Maryam Mohiti <sup>ib</sup>, Mohammadreza Mazidi <sup>ib</sup>, Niccolò Oggioni, David Steen <sup>ib</sup>, and Le Anh Tuan <sup>ib</sup>, *Member, IEEE*

**Abstract**—Local energy communities (LECs) facilitate energy distribution, supply, consumption, storage, and trading for the communities and their members. This article proposes an energy management system (EMS) for optimal heat and power scheduling in LECs. A novel model for the phase-change thermal energy storage (TES) which is applicable in mixed integer linear problems (MILP), is introduced. Furthermore, a risk-averse and risk-seeker EMS is developed that incorporates the integration of TES to optimize electricity and heat scheduling in LECs. The developed EMS doesn't require probability distribution functions of predicted data which makes it valuable in cases with high levels of uncertainties or lack of sufficient historical data. To validate the performance of the proposed TES model, real time studies are conducted on an industrial TES provided by Azelio company. Likewise, the effectiveness and efficiency of the proposed EMS are evaluated on a real LEC at Chalmers University of Technology campus, Gothenburg, Sweden.

**Index Terms**—Electricity and heat scheduling, energy management system, local energy community, phase change thermal energy storage, risk-averse model.

## NOMENCLATURE

### Indices

$t$  Index of time.

### Parameters

$\epsilon^{H,Stir}$  Effectiveness of the heat exchanger of Stirling engine.

$\eta_d/\eta_{ch}$  Charge/discharge efficiency of battery energy storage.

$\eta^{h, TES} / \eta^{h, SB}$

$\eta^{Gen}$

$\epsilon_t^{H,Stir}$

$\eta^{Mec,Stir}$

$\lambda_t^e$

$\lambda_t^h$

$c^{deg}$

$C^L / C^S$

$C^W$

$H_t^{idle, TES}$

$H_t^L$

$H^{Lat}$

$k$

$A$

$M/M1$

$m^{TES}$

$P_t^{PV}$

$P_t^L$

$T_t^a$

$T_t^{CW}$

$T^{L1} / T^{L2}$

$T^{S1} / T^{S2}$

$T^{offset}$

$T_t^{TES,0}$

$V$

$V_t^{HW}$

$T_{min}^{HW}, T_{max}^{HW}$

**Variables**

$\alpha_{pv}, \alpha_{ld}$

$H_t^{ch, TES} / H_t^{dis, TES}$

Efficiency of TES/smart boiler heater.

Efficiency of TES output generator.

Efficiency of Stirling engine thermodynamic cycle.

Mechanical efficiency of Stirling engine.

Electricity spot market price.

District heating variable heat price.

Parameter to emulate degradation cost of battery.

Specific heat of phase change material (PCM) inside TES in in liquid/solid phase.

Specific heat of water.

Idle losses of TES.

Heat demand of LEC.

Latent heat of PCM in TES.

Thermal convection parameter of SB tank.

Area of smart boiler tank.

Big numbers in big M method.

Mass of PCM inside TES tank.

Forecasted PV power.

Forecasted value of electrical power.

Ambient temperature.

Temperature of cold water in smart boiler tank.

Temperature boundaries of PCM liquid phase in TES.

Temperature boundaries of PCM solid phase in TES.

Offset value in enthalpy curve of PCM in TES.

Initial Temperature of PCM inside TES.

Tank volume of smart boiler.

Hot water demand.

Minimum/maximum desired hot water temperature.

Robustness/ opportunity index of PV generation and load demand in IGDT method.

Charge/discharge heat of TES.

Manuscript received 11 August 2023; revised 30 November 2023; accepted 26 December 2023. Date of publication 29 January 2024; date of current version 21 May 2024. Paper 2023-ESC-0952.R1, presented at the 2022 IEEE International Conference on Environment and Electrical Engineering and 2022 IEEE Industrial and Commercial Power Systems Europe (EEEIC / I&CPS Europe), Prague, Czech Republic, Jun. 28–Jul. 01, and approved for publication in the IEEE TRANSACTIONS ON INDUSTRY APPLICATIONS by the Energy Systems Committee of the IEEE Industry Applications Society [DOI: 10.1109/EEEIC/ICPSEurope54979.2022.9854642]. This work was supported by SUNSETS Project within Solar ERANET Program, funded by the Swedish Energy Agency under Project 51197-1. (*Corresponding author: Maryam Mohiti.*)

Maryam Mohiti, Mohammadreza Mazidi, David Steen, and Le Anh Tuan are with the Chalmers University of Technology, 412 96 Gothenburg, Sweden (e-mail: maryamar@chalmers.se; mazadi@chalmers.se; david.steen@chalmers.se; tuan.le@chalmers.se).

Niccolò Oggioni is with the Azelio AB, 111 20 Gothenburg, Sweden (e-mail: nicolo.oggoni@azelio.se).

Color versions of one or more figures in this article are available at <https://doi.org/10.1109/TIA.2024.3359126>.

Digital Object Identifier 10.1109/TIA.2024.3359126

$H_t^{Im,LEC} / H_t^{Ex,LEC}$	Imported/Exported heat to LEC from district heating.
$H_t^{SB}$	Heat input to smart boiler.
$H_t^{R,Stir}$	Residual heat of Stirling Engine.
$P_t^{ch,BES} / P_t^{dis,BES}$	Charge/discharge power of BES.
$n_t^{sh,Stir}, p_t^{Stir}$	Stirling engine shaft speed, pressure, heat source temperature, heat sink temperature.
$T_t^{H,Stir}, T_t^{C,Stir}$	Temperature.
$P_t^{Im,LEC} / P_t^{Ex,LEC}$	Import/export active power to/from LEC.
$PV_t^{Cur}$	Curtailed power of PV.
$P_t^{TES-Stir} / P_t^{in,TES}$	Output/input power of TES.
$Q_t^{TES}$	Enthalpy of TES.
$Q_t^{H,Stir}$	Input heat to thermodynamic cycle of Stirling engine.
$Q_t^{C,Stir}$	Low temperature heat output of thermodynamic cycle of Stirling engine.
$SoC_t$	State of charge of battery energy storage.
$T_t^{TES}$	Temperature of PCM of TES.
$T_t^{HW}$	Hot water temperature of smart boiler tank.
$u_t^{ch,BES} / u_t^{d,BES}$	Binary variables for charge/discharge of battery energy storage.
$u_t^{ch,TES} / u_t^{dis,TES}$	Binary variables for charge/discharge of TES.
$u_t^1 - u_t^5$	Binary variables for linearizing TES characteristic.
$W_t^{Stir}$	Work output of the Stirling engine heat cycle.
$W_t^{M,Stir}$	Mechanical work output of the Stirling engine.
$z_t^{aux1}, z_t^{aux2}, z_t^{aux3}$	Auxiliary variables indicating enthalpy of each region in enthalpy-temperature curve.
<b>Symbol</b>	
$\overline{(\bullet)} / \underline{(\bullet)}$	Maximum/minimum bounds of $(\bullet)$ .
$\widetilde{(\bullet)}$	Uncertain value of variable $(\bullet)$ .
$f_1, f_2, f_3$	Polynomial functions.

## I. INTRODUCTION

THE increasing integration of distributed energy sources (DERs) and the implementation of demand response programs in distribution networks, has highlighted the need of considering them as an entity. To this end the European Commission's has introduced the concept of local energy communities in the EU legislation [1]. LECs are clusters of DERs which collaborate to generate, distribute, and consume energy locally. LECs, with both electricity and heat vectors, offer a comprehensive and integrated approach to energy management. Through combination of renewable resources with efficient storage systems, LECs are able to optimize the utilization of electricity and heat, ensuring a reliable and sustainable energy supply for their members. Indeed, battery energy storage (BES) enable the storing and utilization of surplus electricity, while thermal

energy storage allows for the efficient storing and utilization of excess heat, thereby maximizing the overall energy efficiency and flexibility of the community.

Thermal energy storages are gaining significant attention as one of the most promising ways to enhance flexibility in LECs. This is primarily because TES offers a multitude of advantages, large storage capacity, and cost-effectiveness [2]. As in [3] the role of TESs in energy balancing of wind power in isolated electrical grids are evaluated. Ref. [4] models the combined dispatch of combined heat and power (CHP) units, TES, and heat pump to explore the flexibility provision capability of them. In [5], the LEC participates in both electricity and thermal energy markets by integrating BES and TES in its scheduling. likewise, authors of [6] present a multi objective decision-making framework to determine the optimal scheduling of a LEC incorporated with a TES. In the aforementioned studies, and similarly to many other energy management studies [5], [6], [7], TESs are typically modeled with only the consideration of thermal energy balance and constraints on the maximum stored heat or released heat. These works do not account for the thermodynamic equations of the TES and instead regard the TES as analogous to a BES. Based on the mode of heat transfers, TESs can be categorized in three forms; sensible heat (SH), latent heat (LH) and thermo-chemical heat storage [8]. Each category inherently possesses distinct operational characteristics, which inevitably affect the flexibility they can offer. However, previous studies have treated the difference between sensible heat TESs and latent heat TESs solely based on the thermal energy balance equation. Consequently, the existing modeling approaches fail to accurately reflect the genuine disparities in system performance. In few EMS studies such as [9] and [10], [11] the thermo-dynamic model of the TES is considered. As in [9], [10] the heat transfer processes of the TES with the entransy dissipation thermal resistance model has been considered in the dispatch model of a CHP with a TES [12]. This model is nonlinear and utilizes an iterative procedure to solve the optimization problem. Authors of [11] present an enthalpy-based model to analyze the thermal characteristics of the Phase Change Material (PCM) integrated in the wallboard of a smart building which acts similar to LH TES. These studies assume that the PCM of the TES is constant in the phase change mode and the temperature change of the PCM due to the mixture of solid and liquid phases is not considered. More importantly the TES can be modeled in one working region i.e., latent, or sensible heat. In other words, if the LH TES can provide heat in the solid and liquid phases of the PCM as an SH TES this capacity is not considered. In many industrial LH TESs, the sensible heat regions can constitute a significant portion of the overall heat capacity of the TES and disregarding this energy capacity underestimates the storage capability in providing flexibility. To fill this gap, a novel model for phase change TES is presented in this paper which is based on the enthalpy-temperature equation of TESs. In the proposed model, a more realistic assumption that the PCM melts over an interval rather than a constant temperature, is considered and both the SH and LH regions of the TES are precisely modeled, resulting in a more realistic representation, and enabling the utilization of the TES's full capacity. Likewise, since all heat regions are

modeled, the proposed model can be used for both SH and phase change TESs applications. Furthermore, the model is linearized with the big M method [13], making it applicable in MILPs.

The operation of a LEC requires the implementation of an energy management system (EMS) to optimize electricity and thermal energy scheduling of the available DERs. However, the unpredictable nature of renewable generation and load demand affects the performance of EMS. To tackle this issue, several optimization methods have been developed, namely stochastic optimization (SO) [14], robust optimization (RO) [15], and interval optimization (IO) methods [16]. SO methods are based on probability distribution functions (PDFs) of predicted data which are used to create numerous scenarios with their probabilities [17]. However, the accuracy of SO is dependent on the accuracy of the PDFs, i.e., forecasts, and the number of scenarios. In the real-world application the lack of sufficient data to establish high accuracy forecast methods, not only degrades the prediction, but also results in inaccurate PDFs and a non-optimized solution. In RO methods the worst-case scenario is realized enforcing a conservative and robust costly solution. To deal with this, IO methods namely information gap decision theory (IGDT) method are utilized in the developed EMS of presented paper. The IGDT method only requires forecasted values and lower and upper bands of predicted data which are easier to obtain in real-world application from historical data. Likewise, since in the IGDT method, the optimization problem should neither be solved in different scenarios nor found the worst-case scenario, the computational burden is low. Moreover, IGDT method finds optimal solutions that are immunized against all possible realizations of uncertain variables, unlike SO that provides probabilistic guarantees for constraint satisfaction [18]. In [19], a bilevel optimization approach has been proposed to coordinate the operation of multiple LECs within a system. In the proposed model, the uncertainty of energy demands, renewable power generation, and energy prices are considered using the IGDT method. In [20], optimal scheduling of a residential community with the presence of renewable energy sources and electric vehicles has been modeled considering uncertainties of RESs and EVs using the IGDT method. In the developed EMS, IGDT method is utilized to handle the uncertainties of PV and demand and a pre-specified level of cost is guaranteed.

The performance of the proposed EMS is evaluated on a real LEC at Chalmers University of Technology campus, Gothenburg, Sweden. In this LEC, Azelio TES.POD is virtually connected as a community member [21] as part of the European project SUNSETS [22]. Azelio TES.POD is a TES coupled with a Stirling engine to produce electricity on demand. Likewise, The TES model is validated with a detailed real time model of the TES. In summary the contributions of the paper can be described as:

- 1) A novel enthalpy-temperature-based model for phase change TES is introduced. This model enhances industry applications by simulating PCM melting over an interval, accommodating both sensible and latent heat regions. It provides a more accurate portrayal of TES behavior and performance, enhancing its practical applicability.

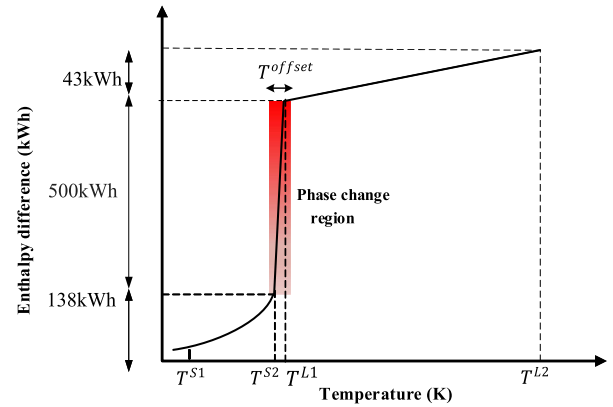


Fig. 1. Enthalpy-temperature curve of Azelio TES.POD Aluminum alloy PCM.

- 2) The nonlinear equality constraints introduced by the TES model are linearized making it applicable to MILP studies.
- 3) The proposed TES model is validated with a detailed real-time model of an industrial TES i.e, Azelio TES.POD.

This paper is organized as follows: In Section II the proposed phase change TES model is introduced. Meanwhile Section III presents the EMS model, and the uncertainty handling approach is described in Section IV. The case study and simulations are conducted in Section V. Finally, conclusions are drawn in Section VI.

## II. PROPOSED LATENT HEAT TES MODEL

Latent heat storages exploit the enthalpy of phase change as the storage mechanism. The storage material namely, phase change material, transfers from solid to liquid and other way around, to release and store heat. As PCM can absorb/release a large amount of energy at an almost constant temperature, therefore, latent heat TESs have a considerably higher energy density compared to sensible heat TESs [2]. Azelio TES.POD is based on Aluminum alloy phase change material and the latent heat is the main portion of its stored heat. However, it can deliver energy in the liquid and solid phases as a sensible heat TES, as well. The enthalpy-temperature relationship of the Aluminum alloy PCM is depicted in Fig. 1 which the amount of energy delivered in each region is indicated.

In theory a eutectic mixture has a defined melting point, and it changes from solid state to liquid state with a constant temperature, however in reality this is seldom the case, and the PCM melts over an interval. The width of this interval can be defined via  $T^{offset}$  as depicted in Fig. 1. In this paper a novel enthalpy-based model for TES is proposed in which the TES can operate in three regions of the enthalpy-temperature curve of Fig. 1 enabling the TES to deliver energy in both sensible and latent heat regions (solid and liquid phase as a sensible heat and phase change region). Likewise, with the proposed model a temperature offset based on Azelio experiments is considered in the latent phase making the model more realistic. With respect to Fig. 1, the enthalpy of the TES is presented as a function of

the temperature in all the phase regions as follows:

$$\begin{aligned} Q_t^{TES} &= \int_{T_t^{TES,0}}^{T_t^{TES}} m^{TES} C^{TES} dT \\ &= m^{TES} C^{TES} (T_t^{TES} - T_t^{TES,0}) \end{aligned} \quad (1)$$

where, depending on the temperature of the PCM ( $T_t^{TES}$ ), the PCM can be in solid, liquid, or latent phase and the specific/latent heat i.e.,  $C^{TES}$  is defined as follows:

$$C^{TES} = \begin{cases} C^L & T^{L1} < T_t^{TES} < T^{L2} \\ C^{Lat} & T^{S2} \leq T_t^{TES} \leq T^{L1} \\ C^S & T^{S1} < T_t^{TES} < T^{S2} \end{cases} \quad (2)$$

The solid and liquid specific heats i.e.,  $C^s$  and  $C^L$  are assumed constant while  $C^{Lat}$  is derived from the slope of the enthalpy-temperature curve of Fig. 1 which is the linearization of the latent heat through the offset interval as follows:

$$C^{Lat} = H^{Lat} / 2T^{offset} \quad (3)$$

Note that  $m^{TES}$  is the mass of PCM of the TES tank and is constant. The enthalpy difference equals to the charge and discharge heat and idle losses in case of no charge/discharge as (4). Equation (4) is transformed to the discrete form for time steps of  $\Delta t$  as (5):

$$m^{TES} C^{TES} \frac{dT_t^{TES}}{dt} = H_t^{ch, TES} - H_t^{dis, TES} - H_t^{idle, TES} \quad (4)$$

$$\begin{aligned} m^{TES} C^{TES} (T_{t+1}^{TES} - T_t^{TES}) \\ = (H_t^{ch, TES} - H_t^{dis, TES} - H_t^{idle, TES}) \Delta t \end{aligned} \quad (5)$$

Since  $C^{TES}$  is correlated to the temperature based on (2), (5) is not linear, Therefore, it is converted to a MILP with the big M method [13] with the set of equations of (6)–(23) to make 3it applicable in optimization and energy management studies. The auxiliary variables  $z_t^{aux1}$ ,  $z_t^{aux2}$ ,  $z_t^{aux3}$  will indicate the enthalpy in each of the regions of the enthalpy-temperature curve of Fig. 1 while binary variables  $u_t^1 - u_t^5$  enforce them to have values in only one region per timestep.

$$\begin{aligned} z_t^{aux1} + z_t^{aux2} + z_t^{aux3} = (H_t^{ch, TES} - H_t^{dis, TES} \\ - H_t^{idle, TES}) \Delta t \end{aligned} \quad (6)$$

$$-Mu_{t,i}^4 \leq z_t^{aux1} \leq Mu_{t,i}^4 \quad (7)$$

$$\begin{aligned} m^{TES} C^L (T_{t+1}^{TES} - T_t^{TES}) - M(1 - u_t^4) \leq z_{t,i}^{aux1} \\ \leq m^{TES} C^L (T_{t+1}^{TES} - T_t^{TES}) + M(1 - u_t^4) \end{aligned} \quad (8)$$

$$T^{L1} - M(1 - u_t^4) \leq T_t^{TES} < T^{L2} \quad (9)$$

$$-Mu_t^5 \leq z_t^{aux2} \leq Mu_t^5 \quad (10)$$

$$\begin{aligned} m^{TES} C^{Lat} (T_{t+1}^{TES} - T_t^{TES}) - M(1 - u_t^5) \leq z_t^{aux2} \\ \leq m^{TES} C^{Lat} (T_{t+1}^{TES} - T_t^{TES}) + M(1 - u_t^5) \end{aligned} \quad (11)$$

$$T^{S2} - M(1 - u_t^5) \leq T_t^{TES} \leq T^{L1} + M(1 - u_t^5) \quad (12)$$

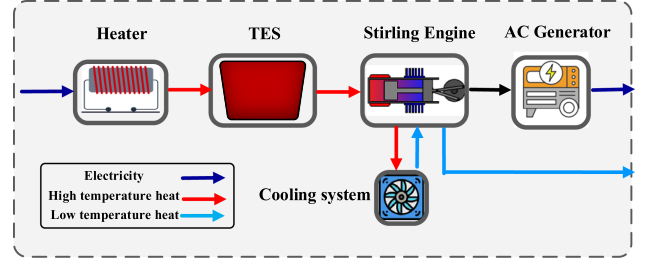


Fig. 2. Schematic diagram of the Azelio TES.POD.

$$-Mu_t^1 \leq z_t^{aux3} \leq Mu_t^1 \quad (13)$$

$$\begin{aligned} m^{TES} C^S (T_{t+1}^{TES} - T_t^{TES}) - M(1 - u_t^1) \leq z_t^{aux3} \\ \leq m^{TES} C^S (T_{t+1}^{TES} - T_t^{TES}) + M(1 - u_t^1) \end{aligned} \quad (14)$$

$$T^{S1} < T_t^{TES} \leq T^{S2} + M(1 - u_t^1) \quad (15)$$

$$(T^{S2} - T_{t-1}^{TES}) / M1 \leq u_t^1 \quad (16)$$

$$(T_{t-1}^{TES} - T^{S2}) / M1 \leq u_t^2 \quad (17)$$

$$u_t^1 + u_t^2 = 1 \quad (18)$$

$$(T_t^{TES} - T^{L1}) / M1 \leq u_t^4 \quad (19)$$

$$(T^{L1} - T_t^{TES}) / M1 \leq u_t^3 \quad (20)$$

$$u_t^4 + u_t^3 = 1 \quad (21)$$

$$u_t^5 \leq u_t^3, u_t^5 \leq u_t^2, \quad (22)$$

$$u_t^2 + u_t^3 - 1 \leq u_t^5 \quad (23)$$

Azelio TES.POD is coupled with a Stirling engine and generator to deliver power on demand. The Aluminum alloy is heated by an electrical heater to phase change. The heat of the TES is transferred to the Stirling engine through a heat transfer fluid, on demand. The Stirling engine drives a generator for electricity, and the low temperature (55–65 °C) residual heat of the Stirling engine can be utilized through the heat to energy (H2E) technology. The schematic of the TES.POD is depicted in Fig. 2. The charged power of the TES through the electrical heater can be obtained as follows:

$$H_t^{ch, TES} = \eta^{h, TES} P_t^{in, TES} \quad (24)$$

The charge and discharge power of the TES are constrained by their operational limit represented in (25)–(27). Since the charge and discharge circuits of the TES are decoupled simultaneous charge/discharge is not possible, hence, (28) is added to prevent simultaneous charge/discharge.

$$P_t^{in, TES} \leq u_t^{ch, TES} \overline{P_t^{in, TES}} \quad (25)$$

$$0 \leq H_t^{ch, TES} \leq u_t^{ch, TES} \overline{H_t^{ch, TES}} \quad (26)$$

$$0 \leq H_t^{dis, TES} \leq u_t^{dis, TES} \overline{H_t^{dis, TES}} \quad (27)$$

$$u_t^{ch} + u_t^{dis} \leq 1 \quad (28)$$

The discharged heat of the TES is directed through a Stirling engine with a heat transfer fluid (29). The work as output of the thermodynamic cycle of the Stirling engine, is related with thermodynamic-work efficiency ( $\eta^{W, TES}$ ) and the residual heat is correlated to the input heat with the heat effectiveness of the heat exchanger ( $\epsilon^{H, TES}$ ). Note that functions for  $\eta^{W, Stir}$  and  $\epsilon^{H, TES}$  are derived, with fitting experimental real data to polynomial functions to  $Q_t^{H, Stir}$ ,  $Q_t^{C, Stir}$ ,  $W_t^{Stir}$ , and  $Q_t^{loss, Stir}$  as (30)–(32) and collected from Azelio. The dynamic values of  $\eta^{W, Stir}$  and  $\epsilon^{H, TES}$  correlates them to the heatsink temperature, heat source temperature, speed and pressure of the Stirling engine with respect to (30)–(32) at every timestep. Equation (33) presents the energy balance in the thermo-dynamic cycle of the Stirling engine. The heatsink temperature is considered to follow the ambient temperature by (34) while the heat source temperature is assumed to remain constant. The mechanical work output of the Stirling engine is linked to its input heat i.e., discharged heat from the TES (35) while its losses is considered by (36). The residual heat of the Stirling Engine can be calculated based on (37). The generator produces electricity with the efficiency  $\eta^{Gen}$  (38). The efficiency of the inverter is considered in  $\eta^{Gen}$ . The operational limits of the Stirling engine are enforced by (39) and (40).

$$Q_t^{H, Stir} = H_t^{dis, TES} \quad (29)$$

$$Q_t^{H, Stir} = f_1 \left( n^{sh, Stir}, p^{Stir}, T^{H, Stir}, T_t^{C, Stir} \right) \quad (30)$$

$$Q_t^{C, Stir} = f_2 \left( n^{sh, Stir}, p^{Stir}, T^{H, Stir}, T_t^{C, Stir} \right) \quad (31)$$

$$W_{t,i}^{Stir} = f_3 \left( n^{sh, Stir}, p^{Stir}, T^{H, Stir}, T_t^{C, Stir} \right) \quad (32)$$

$$Q_t^{H, Stir} = Q_t^{C, Stir} + W_t^{Stir} + Q_t^{loss, Stir} \quad (33)$$

$$T_t^{C, Stir} = T_t^a + 20 \quad (34)$$

$$W_t^{Stir} = \eta_t^{W, Stir} Q_t^{H, Stir} \quad (35)$$

$$W_t^{M, Stir} = \eta^{Mec, Stir} W_{t,i}^{Stir} \quad (36)$$

$$H_t^{R, Stir} = \epsilon_t^{H, Stir} Q_t^{H, Stir} \quad (37)$$

$$P_t^{TES-Stir} = \eta^{Gen} W_t^{M, Stir} \quad (38)$$

$$u_t^{dis, TES} \overline{H_t^{R, Stir}} \leq H_t^{R, Stir} \leq u_t^{dis, TES} \overline{H_t^{R, Stir}} \quad (39)$$

$$u_t^{dis, TES} \overline{W_t^{Stir}} \leq W_t^{Stir} \leq u_t^{dis, TES} \overline{W_t^{Stir}} \quad (40)$$

### III. ENERGY MANAGEMENT SYSTEM MODEL

In this section the EMS model and its components are described. The objective function is:

$$\begin{aligned} \text{Min} \sum_t \lambda_t^e \left( P_t^{Im, LEC} - P_t^{Ex, LEC} \right) + c^e P_t^{Im, LEC} \\ + \sum_t \lambda_t^h \left( H_t^{Im, LEC} - H_t^{Ex, LEC} \right) \\ + c^{H, var} H_t^{Im, LEC} + c^{H, fixed} \end{aligned}$$

$$+ \sum_t c^{cur} PV_t^{Cur} + \sum_t c^{deg} \left( P_t^{ch, BES} + P_t^{dis, BES} \right) \quad (41)$$

The first term represents the cost of exchanging active power with the distribution network.  $\lambda_t^e$  denotes the spot price plus taxes, while  $c^e$  refers to the network tariff (a fixed fee for utilizing the network) when the LEC imports energy. The second term accounts for the cost of heat exchange with the district heating system, including the cost of energy exchange and the power cost. The distribution system operator charges district heating consumers based on  $c^{H, var}$  for the peak power input, and  $c^{H, var}$  as a fixed annual cost scaled to an hourly value. The third term presents the cost of PV curtailment. To prevent repeated charging and discharging of the BESS, the fourth term is included to simulate the degradation cost of the BESS. The TES, on the other hand, does not have any degradation cost associated with it [21].

#### A. Constraints on BESS

The BESS is charged and discharged considering the following constraints:

$$0 \leq P_t^{ch, BES} \leq u_t^{ch, BES} \overline{P_t^{ch, BES}} \quad (42)$$

$$0 \leq P_t^{d, BES} \leq u_t^{d, BES} \overline{P_t^{d, BES}} \quad (43)$$

$$u_t^{ch, BES} + u_t^{d, BES} \leq 1 \quad (44)$$

$$SOC_t = SOC_{t-1} + \Delta t \left( P_t^{ch, BES} \eta_{ch} - P_t^{d, BES} / \eta_d \right) \quad (45)$$

$$\underline{SOC}_t \leq SOC_t \leq \overline{SOC}_t \quad (46)$$

(42) and (43) limit the maximum charge and discharge power of the BES, while (44) prevents simultaneous charge and discharge of it. The BES SOC is updated in each timestep by (45) and its minimum and maximum is constrained by (46).

#### B. Constraints on Smart Boiler

A water storage tank supplies hot water demand of the buildings. Electricity can be fed to the smart boiler heater to produce heat, or it can receive heat through a heat exchanger directly by the heat network. The residual heat from Azelio TES utilizing its H2E technology, or the input heat from the district heating system, can be directed to the smart boiler via the heat exchanger, represented by (47). The active electricity power of the boiler serves as input to a controllable heater with the efficiency of  $\eta^{h, SB}$ . It is assumed that the water storage remains consistently full, with any consumed hot water being replaced by an equal volume of cold water in each time interval [8]. The temperature of the water storage can be calculated using (48). It should be noted that the equilibrium temperature of the storage water, resulting from the combination of cold input water and the remaining hot water in the storage, can change due to the replenishment of hot water consumed by the user and thermal convection, where heat is lost through the tank's exterior walls

to the surrounding environment.

$$H_t^{SB} = \eta^{h,SB} \cdot P_t^{SB} + H_t^{SB-H} \quad (47)$$

$$T_{t+1}^{HW} = [V_t^{HW} \cdot (T_t^{CW} - T_t^{HW} + V \cdot T_t^{HW}) / V + H_t^{SB} / VC^W - kA (T_t^{HW} - T_t^a) / VC^W] \quad (48)$$

### C. Constraints on Electrical and Heat Power Balance

The electrical load demand of the LEC should be supplied by resources and the main grid which is considered as (49). The heat demand is composed of hot water demand and space heating demand, which is supplied by the residual heat of Azelio TES, boiler and district heating as in (50).

$$P_t^{Ex,LEC} - P_t^{Im,LEC} = P_t^{PV} + P_t^{d,BES} + P_t^{TES-Stir} - P_t^{in,SB} - P_t^{ch,BES} - P_t^{in,TES} - P_t^L - PV_t^{cur} \quad (49)$$

$$H_t^{Ex,LEC} - H_t^{Im,LEC} = H_t^{R,TES} - H_t^{SB} - H_t^L \quad (50)$$

### D. Power Exchange Limits

The exchanged electrical power and heat with the upstream grid is constrained by (51) and (52). (53) prevents simultaneously import and export to the grid:

$$0 \leq P_t^{Im,LEC} \leq u_t^{Im} \cdot \overline{P_t^{Im,LEC}} \quad (51)$$

$$0 \leq P_t^{Ex,LEC} \leq u_t^{Ex} \cdot \overline{P_t^{Ex,LEC}} \quad (52)$$

$$u_t^{Im} + u_t^{Ex} \leq 1 \quad (53)$$

## IV. UNCERTAINTY HANDLING USING IGDT METHOD

The load demand and PV generation can be forecasted based on historical data and weather prediction models as described in [23]. However, the forecast models are not perfect and are associated with inaccuracy. Thus, the model should be optimized under uncertainty. In this section, first the IGDT method is presented to address the risk of uncertainties from renewable generation and load demand. Then, the EMS based on the risk-averse (RA) and risk-seeker (RS) strategies are formulated.

### A. IGDT Method

The IGDT method determines the optimal robust region (RR) for each uncertain variable to increase the robustness against uncertainty or decrease the cost. The modeling approach includes two distinct formulations, namely the RA strategy for the robustness-based EMS and the RS strategy for the opportunity-based EMS. The RA strategy aims to achieve a balance between minimizing uncertainty with accepting a higher operation cost for the LEC to enhance robustness of scheduling. This can be formulated as follow:

$$\text{Max } (\alpha_{pv}, \alpha_{ld}) \quad (54)$$

$$TOC \leq \overline{TOC} \times (1 + UB) \quad (55)$$

$$(1) - (40), (42) - (50) \quad (56)$$

$$\begin{aligned} TOC = & \sum_t \lambda_t^e \left( P_t^{Im,LEC} - P_t^{Ex,LEC} \right) + c^e P_t^{Im,LEC} \\ & + \sum_t \lambda_t^h \left( H_t^{Im,LEC} - H_t^{Ex,LEC} \right) \\ & + c^{H,var} H_t^{Im,LEC} + c^{H,fixed} + \sum_t c^{cur} PV_t^{Cur} \\ & + \sum_t c^{deg} \left( P_t^{ch,BES} + P_t^{dis,BES} \right) \end{aligned} \quad (57)$$

$$\widetilde{P}_t^L = (1 + \alpha_{ld}) P_t^L, \alpha_{ld} \geq 0 \quad (58)$$

$$\widetilde{P}_t^{PV} = (1 - \alpha_{pv}) P_t^{PV}, \alpha_{pv} \geq 0 \quad (59)$$

The RS strategy focuses on reducing operation cost using deviations of uncertain variables, even if the scheduling involves a greater risk. This can be formulated as follows:

$$\text{Min } (\alpha_{pv}, \alpha_{ld}) \quad (60)$$

$$TOC \leq \overline{TOC} \times (1 - UB) \quad (61)$$

$$(1) - (40), (42) - (50) \quad (62)$$

$$(57) \quad (63)$$

$$\widetilde{P}_t^L = (1 - \alpha_{ld}) P_t^L, \alpha_{ld} \geq 0 \quad (64)$$

$$\widetilde{P}_t^{PV} = (1 + \alpha_{pv}) P_t^{PV}, \alpha_{pv} \geq 0 \quad (65)$$

The conservatism degree of the optimal scheduling against uncertain variables can be controlled through a definite  $UB$ . Note that the developed RA and RS based EMSs in (54)–(65) are multi-objective optimization problems which can be solved using the augmented  $\varepsilon$ -constraint method. Mathematical details of the augmented  $\varepsilon$ -constraint method are given in [24].

## V. CASE STUDY

### A. Test System

The proposed EMS is tested on a LEC located at Chalmers University of Technology campus which its schematic is shown in Fig. 3. The LEC consists of a smart building and campus facilities i.e., PV and loads. The DERs of the smart building are PV, Lithium-ion battery, smart boiler, and Azelio TES.POD. The boiler and Azelio TES are virtually connected to the LEC as they are located at Åmål, Sweden and Patras, Greece tests sites, respectively. The LEC is connected to the electricity distribution network and district heating, facilitating exchange of both electricity and heat. The data of DERs are given in Table I. Likewise, Fig. 4 shows the forecasted hourly load demand, PV generation, and electricity spot prices, which represent real data for a day in August 2022. The district heating price remains constant throughout each month and is considered to be 0.1 SEK/kWh for the month of August. The outdoor temperature and hot water demand of the LEC are depicted in Fig. 5. Note that the hot water temperature can vary between 55 °C to 75 °C .

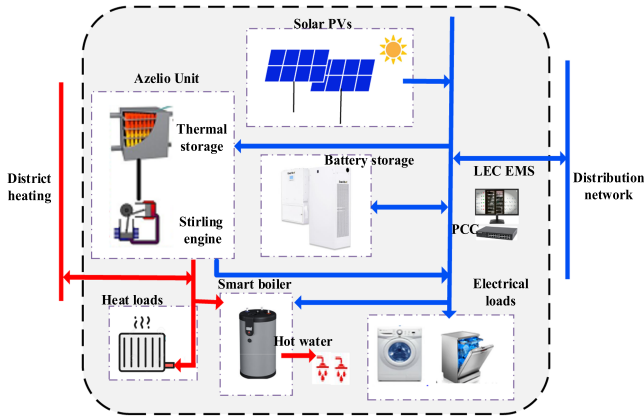


Fig. 3. Schematic of LEC located at Chalmers campus.

TABLE I  
DATA OF THE DERS IN LEC

	Parameter	Value
BES	$\eta^d, \eta^{ch}$	0.95, 0.95
	$SOC_t, SOC_t (p.u)$	0.2, 0.9
	$P_t^{d,BES}, P_t^{ch,BES} (kW)$	100, 100
	$c^{deg} (SEK/kWh)$	0.01
SB	$kA (W/^\circ C), C_w (kJ/kg^\circ C)$	6, 4.18, 600
	$V (lit)$	
	$T^{CW} (^\circ C)$	10
Azelio TES	$T_t^{HW}, T_t^{HW} (^\circ C)$	60, 75
	$\eta^{h, TES}, m^{TES} (kg)$	0.95, 3960
	$C^L, C^S, (kJ/kg^\circ C)$	1.1, 1.224
	$H^{Lat} (kJ/kg)$	477.689
	$T^{S1}, T^{S2}, T^{S1} (K)$	823, 849.5, 850.5, 863
	$H_{t,i}^{idle, TES}, P_{t,i}^{in, TES} (kW)$	2.4, 100
	$H_{t,i}^{dis, TES}, H_{t,i}^{dis, TES} (kW)$	11, 40
	$H_{t,i}^{ch, TES} (kW)$	95
	$\eta^{Mec, Stir}, \eta^{Gen}$	0.82, 0.94
	$H_{t,i}^{R, Stir}, H_{t,i}^{R, Stir} (kW)$	4, 20
	$W_{t,i}^{Stir}, W_{t,i}^{Stir} (kW)$	4.6, 16

### B. Simulation Results

The results of the single objective RA and RS based EMS for robustness and opportunity indexes are presented in Fig. 6. It can be observed that in the RA strategy, as the robustness index increases, the total operation cost also increases to provide more robustness against forecast errors of PV generation and load demand. On the other hand, in the RS strategy, with increasing the opportunity index, total operation cost reduces. This implies that there is an availability of more PV generation or less load demand in real-time compared to their predictions. Moreover, the results indicate that variations of  $\alpha_{pv}$  are larger than  $\alpha_{ld}$  which is due to the low penetration of PV in the LEC. Hence, in the studied LEC, the accuracy of load prediction is more significant compared to the prediction of PV generation.

The Pareto optimal frontier of robustness and opportunity indexes with solving multi-objective RA and RS based EMS for  $UB = 5\%$  are obtained and illustrated in Figs. 7 and 8, respectively. Likewise, the best compromise solution of each

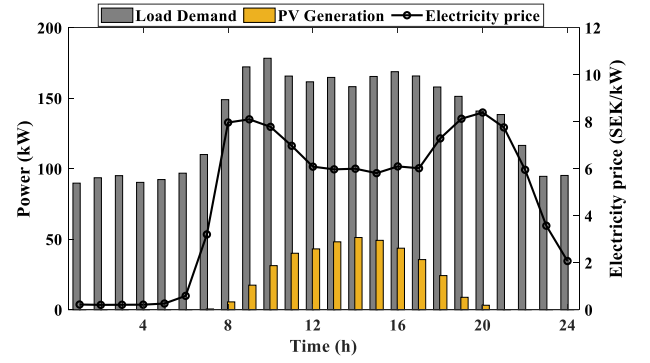


Fig. 4. Hourly forecasted load demand, PV generation, and spot market electricity price.

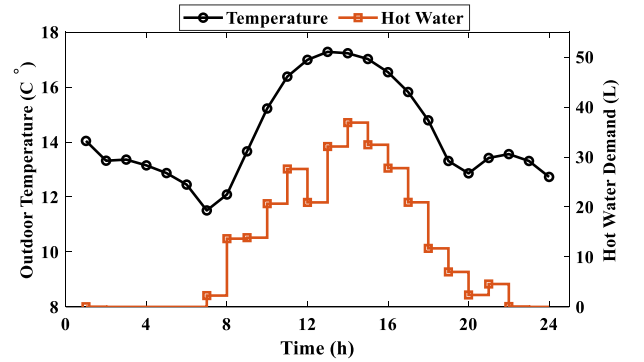
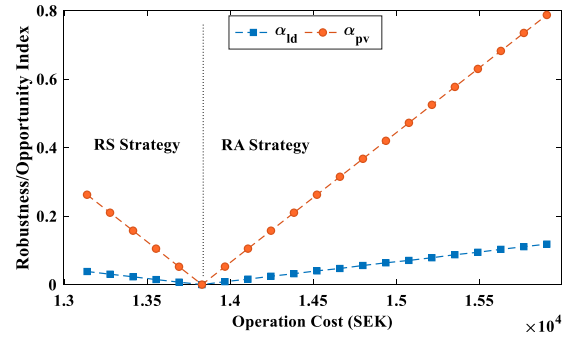
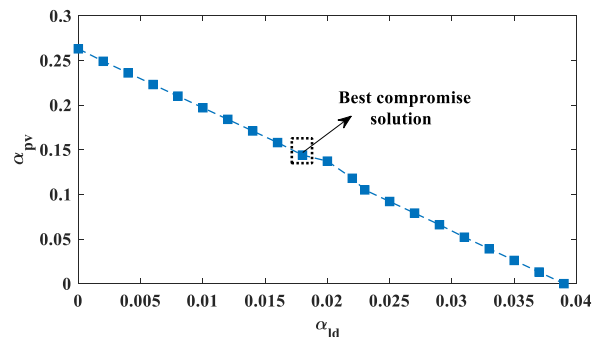


Fig. 5. Hourly outdoor temperature and hot water demand.

Fig. 6. Variations of  $\alpha_{ld}$  and  $\alpha_{pv}$  versus total operation cost in the the single objective RA and RS based EMS.Fig. 7. Pareto frontier in RA strategy with  $UB = 5\%$ .

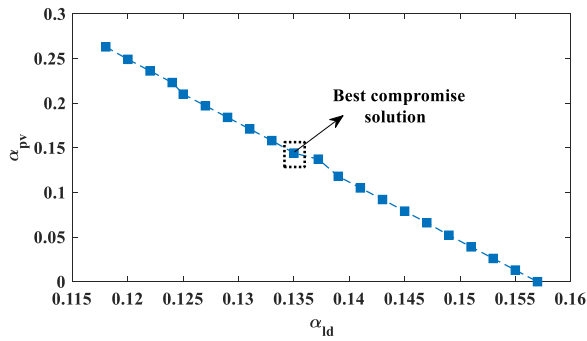
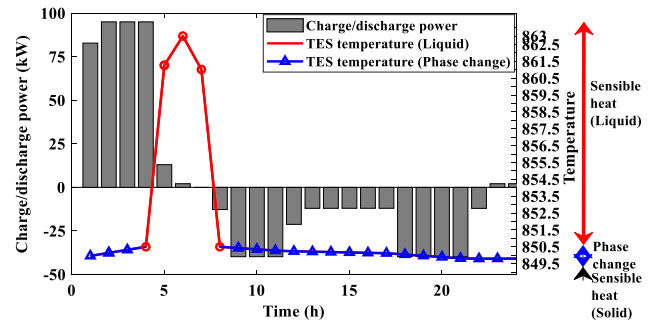

 Fig. 8. Pareto frontier in RS strategy with  $UB = 5\%$ .


Fig. 11. Temperature of TES and charge/discharge profile.

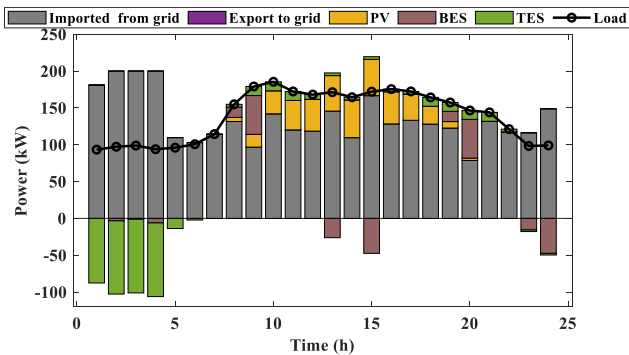


Fig. 9. Optimal power scheduling of LEC in RA strategy.

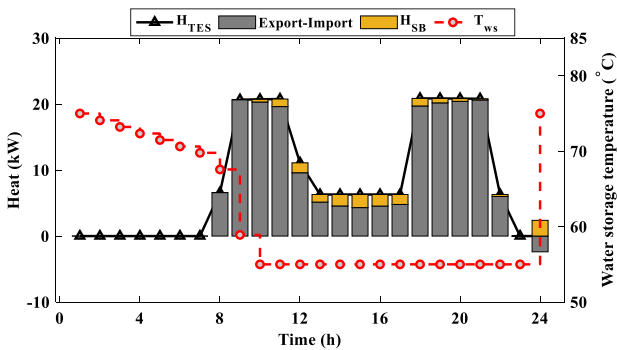


Fig. 10. Optimal heat scheduling of LEC and SB temperature in RA strategy.

strategy is indicated which is acquired by applying the fuzzy set theory. As can be seen, the scheduling is robust against 1.8% of load demand increment and 14.4% of PV generation decrement. Likewise, operation cost of the LEC can be reduced by 5% with 13.3% of load demand decrement and 14.4% of PV generation increment.

Due to the space limit, only the optimal power and heat scheduling results for the best compromise solution of RA strategy are shown in Figs. 9 and 10, respectively. As can be observed, the BESS and TES units are discharged during high-price hours (8:00–12:00, 18:00–21:00) and charged during low-price hours (1:00–5:00, 23:00–24:00). This strategy enables flexibility in terms of energy arbitrage for the LEC. The TES.POD residual heat provides heat for the LEC in most hours. A portion of

this heat is allocated for meeting the hot water demand through the SB, while the excess heat is exported to the district heating system for additional revenue. However, during hours 23:00 and 24:00, when the TES.POD does not provide residual heat due to not being discharged during these hours, the heat requirement for the SB is fulfilled by importing heat from the district heating system. Azelio TES's H2E technology efficiently harnesses the otherwise wasted residual heat from the TES unit, contributing to an overall improvement in the energy efficiency of the LEC. As observed, the SB does not consume heat during the initial hours, leading to a decrease in its temperature to the lower permissible bound of 55 °C. From hours 11:00 to 23:00, the SB utilizes heat to compensate for its losses and maintain the temperature at the same level. At hour 24:00, additional heat is used to increase the temperature back to its initial value, as forced by the optimization process. It's worth noting that since the prices of district heat vary monthly but remain constant daily, the specific hour at which the SB is charged more does not impact the overall operation.

Fig. 11 depicts the charge/discharge profile and the PCM temperature of the TES system. It is evident that the TES charges during low price hours and discharges during high price hours. As the TES charges, the temperature rises from its initial value, transitioning from the phase change region to the liquid sensible heat region. Subsequently, during discharge at later hours of the day, the temperature decreases, re-entering the phase change region. Notably, the sensible heat region exhibits a significant temperature change despite a relatively small enthalpy change, whereas in the phase change region a large amount of heat corresponds to a minimal temperature change. It is noteworthy to highlight that unlike previous studies, the proposed model considers not only all enthalpy-temperature regions but also the interval in which the PCM undergoes melting. This comprehensive approach enhances the accuracy and effectiveness of the model compared to earlier research.

### C. Verification of the IGD-T Performance

To check the robustness and opportuneness of the proposed EMS, Monte Carlo Simulations (MCS) are conducted. To this end, 1000 profiles of load demand and PV generation are generated assuming normal distributions for forecasting errors. Then, the EMS is solved for each scenario. The histogram of resulting operation costs is shown in Fig. 12. It is evident that with respect

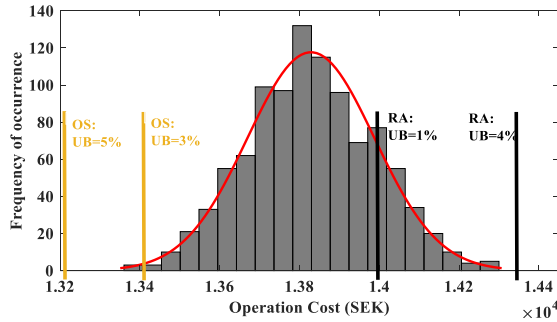


Fig. 12. Histogram of LEC operation costs using the proposed IGDT based approach and MCS.

TABLE II  
COMPARISON OF THE IGDT-BASED MODEL WITH SO-BASED AND RO-BASED MODELS

Comparison indices	IGDT	SO	RO
Total operation cost (SEK)	14590 (99.49%)	14388 (98.11%)	14665 (100%)
PV curtailment (kWh)	0.024	2.992	0.245
Expected cost (SEK)	14356	14130	14410
Standard deviation (SEK)	397.95	2638.12	518.71
Robustness level (%)	99.9	86.5	97.6
CPU time (Seconds)	18 (5.63%)	320 (100%)	146 (46.56%)

to the average value of the MCS, each  $UB$  could lead to either an economic, conservative, or opportunistic scheduling for the LEC. For instance, RA strategies with a  $UB$  of 1% are economic, while those with a  $UB$  of 4% are conservative. Similarly, RS strategies with a  $UB$  of 3% are economic, whereas those with a  $UB$  of 5% are conservative. Therefore, from Fig. 12 one can conclude that a greater distance of  $UBs$  from the MCS average values signifies more conservative or opportunistic strategies, whereas  $UBs$  that lead to economic strategies tend to be closer to the MCS average values. This fact can be used by the operators of the LEC to determine the preferred  $UB$  according to their strategy and accuracy of predictions.

#### D. Comparative Analysis With Existing Uncertainty Handling Methods

To compare the performance of the IGDT method with existing uncertainty handling methods, SO and RO methods are used to implement the proposed model. The SO model is based on which is a two-stage stochastic optimization problem. The MCS technique is employed to generate 10000 profiles of load demand and PV generation. Then, K-means clustering algorithm is applied to decrease the number of generated scenarios to 25. The RO model is based on [25], aims to ensure the robustness of solution with probability greater than 95%, the budget of uncertainty is set to 8 in this study.

To compare the above methods, the day-ahead schedules obtained by each model are analyzed by MCS against various realizations of uncertainties as described. The summary of the results is given in Table II. As can be seen, total operation cost in IGDT-based model is slightly higher than SO (1.4% increase)

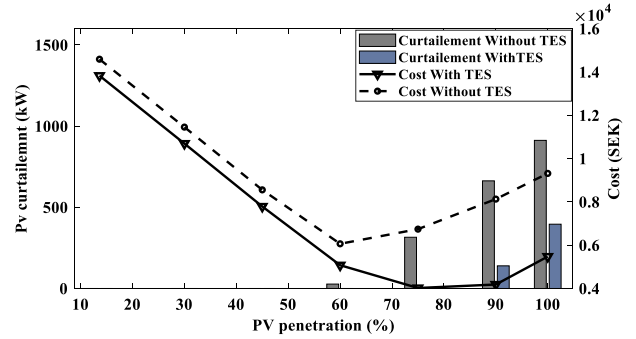


Fig. 13. Sensitivity analysis of cost and PV curtailment with PV penetration of LEC with and without TES.

and is 0.5% lower than that obtained by RO. Likewise, the IGDT-based model demonstrates the most efficient utilization of PV generation, as evidenced by its lowest PV curtailment. Although the expected cost of the IGDT-based model is higher than that of the SO-based model, it has the lowest standard deviation, indicating minimal variation in real-time costs. Robustness level is the ratio of Violated scenarios to all scenarios. Violated scenarios occur when the provided schedule fails to maintain the total operation cost below the predefined value in the IGDT-based model. Referring to Table I, it is clear that the IGDT-based model has the best robustness level. Likewise, the IGDT-based model stands out as the most efficient method in terms of computational time, a highly desirable feature for real-world applications.

#### E. Sensitivity Analysis on the PV Hosting Capacity of LEC

To investigate the role of Azelio TES on enhancing the PV hosting capacity of the LEC, a sensitivity analysis is carried out, consisting of two distinct cases. In the first case, no TES is employed, while in the second case, Azelio TES is dispatched. Fig. 13 illustrates the levels of PV curtailment and operational costs incurred by the LEC at various PV integration levels: 15% (baseline)-100%. Up to a PV penetration level of 45%, neither of the cases experience PV curtailment. However, at PV penetration levels of 60% and 75%, a notable distinction arises between the two cases. In case 1, without any TES, PV curtailment occurs, whereas in case 2, the utilization of Azelio TES eliminates PV curtailment by leveraging its flexibility capabilities. This can be further elaborated in Fig. 14 which showcases the charge profile of the TES during a PV penetration level of 75%. During peak PV hours (from 12:00 to 16:00), the TES is charged to prevent PV curtailment. In higher PV penetration levels, both cases experience PV curtailment to some extent; however, the implementation of Azelio TES still plays a significant role in reducing the amount of curtailment. It is important to note that even with the TES, complete avoidance of PV curtailment in high penetration scenarios is unachievable due to the limited capacity of the TES, which restricts further charging during periods of high PV generation. Furthermore, the cost analysis reveals that case 2 consistently exhibits lower expenses across all PV penetration levels compared to case 1. This cost disparity

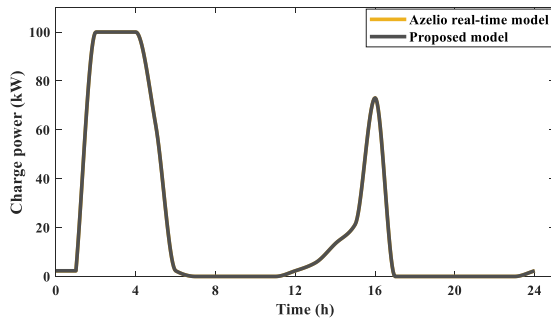


Fig. 14. Validation of proposed model with Azelio real-time model – Charge operation.

is primarily attributed to the contribution of the TES in enabling energy arbitrage and generating income for the LEC. As PV penetration levels increase, the cost difference between case 1 and case 2 becomes more pronounced. This is because the TES not only provides income through energy arbitrage but also helps mitigate the costs associated with PV curtailment in high penetration scenarios.

#### F. Validity of the TES Model

The main objective of this section is to investigate the validity of the proposed model for the TES with Azelio real time study models. Although the proposed model is a novel enthalpy-temperature based model for TES which also considers the liquid and solid phases of the TES, however, to make it tractable in optimization studies some simplifications are made comparing to real-time study models. For example, the TES in this study is modelled as a non-dimensional mass of PCM, while Azelio models the TES as a discretized 2D-axi-symmetric. Additionally, the properties of the cooling system fluid and the heat transfer fluid are considered constant and independent from temperature, which is not the case in the Azelio in-house model, where the fluid property models are temperature dependent. Another significant difference lies in the Stirling engine controller, which Azelio has designed to regulate both engine speed and pressure as function of requested power output, heat source and heat sink temperature, according to a detailed engine mapping. On the other hand, the proposed TES.POD model used in this study operates the engine with less strict boundaries.

To validate the assumptions made in the linearized model, the proposed model's results are compared to what the Azelio in-house TES.POD model would produce under the same assumptions and inputs. The optimized charge and discharge profiles resulted from 75% PV penetration of Fig. 14 in the proposed linearized model are shown in Figs. 15 and 16. Note that there is not a direct match between optimization inputs and the Azelio in-house model, therefore the following adjustments were considered:

- The “Charge power” in Fig. 14 is the available charging power for the TES.POD, not necessarily the actual power input. The charging power controller may curtail the power as the TES approaches full charge to prevent overheating of the PCM. The “Discharge power” in Fig. 15 represents the required power at the AC generator output. The TES.POD discharge controller adjusts the engine setpoint

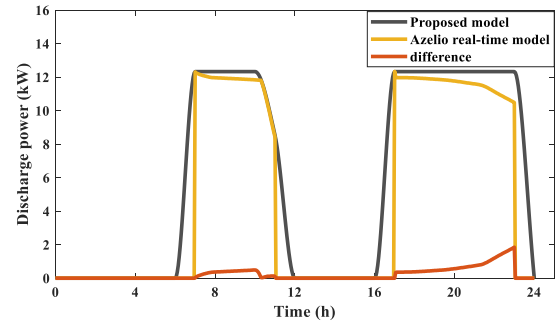


Fig. 15. Validation of proposed model with Azelio real-time model – discharge operation.

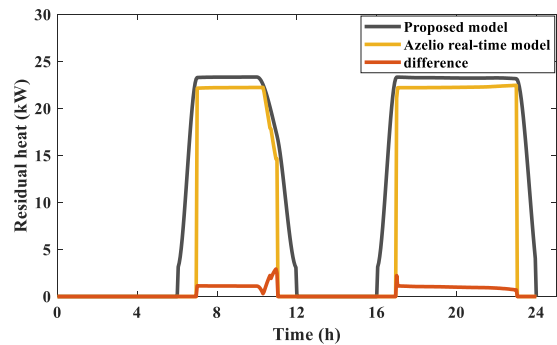


Fig. 16. Validation of proposed model with Azelio real-time model – discharge operation, residual heat of Azelio TES.

(pressure and speed) to match the power request at the inverter output. To account for power losses downstream of the AC generator, the proposed linearized model power request was reduced. However, the temperature limits considered in the model of Section III prevent overcharging or over-discharging.

- The optimization TES model was initialized at 849.8 K, which corresponds to setting the Azelio in-house 2D model to homogeneously 833 K as the real-life measured temperature is the temperature of the outer surface of the tank, close to the tank lid.
- Regarding the residual heat profile, it was necessary to increase the proposed model's residual heat output by 3 kW, representing the cooling needs of the Stirling engine oil, before comparing it to the Azelio in-house output.

Results from the validation process are shown in Figs. 14, 15 and 16 for the charging power, discharging power and residual heat, respectively. Fig. 14 clearly shows an exact match between the charging power profile calculated by the proposed linearized model for this scenario and what the Azelio TES.POD model is able to charge in the TES. More significant differences can be noted during the discharge operation (Fig. 15). Here, the most significant difference is seen at the start and stop of each discharge: the Azelio in-house model starts the discharging one hour later than what the proposed linearized model simulated, and it finishes one hour earlier. This is caused purely by different modelling approaches. The proposed linearized model simulates with a fixed hourly timestep, while the Azelio in-house modelling software uses a solver with variable timestep, which depends on the complexity of the computational state, and

is always shorter than 30 s. The proposed linearized model charging power and discharging power request profiles are then automatically linearly interpolated by the solver to adjust to the variable timestep. Consequently, there are timesteps when both the charging power and discharging power request are not null, e.g., between the 6<sup>th</sup> and 7<sup>th</sup> hour, as seen in Fig. 15 Azelio TES.POD model always prioritises charging over discharging and therefore it triggers the discharge start only when the charging power has reached 0 kW, e.g., after the 7<sup>th</sup> hour from the start in Fig. 15.

Similarly, the same situation takes place once again when the discharge is stopped, with the Azelio model stopping the discharge one hour earlier than in the proposed linearized model. As this difference is independent from the quality of the proposed model and irrelevant to the validation of it, the power difference between Azelio and the proposed model outputs was calculated only when Azelio TES.POD model power output is not null. The Azelio TES.POD model supplies generally less power than the proposed linearized model, with a power difference that increases as temperature of the storage decreases. This is due to the highly detailed TES model in use at Azelio, which replicates the different temperatures inside and outside the PCM. As the PCM is cooled from the outside, the outermost layers of the PCM are the first to solidify, meaning that the same heat flow will be transferred to the Stirling engine at lower temperature due to the thermal gradient across the solid zone. This causes a decrease in the electrical power output. This power tapering effect is most accentuated at lower temperatures', e.g., between the 21<sup>st</sup> and 24<sup>th</sup> hour in Fig. 15. Given the charge and discharge profile presented in Figs. 14 and 15, the PCM was not melted enough to supply constant temperature heat for the next 7 hours and, as a consequence, the TES.POD would experience tapering in the last couple of hours of discharge. This behaviour is completely absent in proposed model as here the TES is considered a non-dimensional mass always at homogenous temperature. However, the proposed model delivers, on average, only +0.56 kW electricity more at generator output than the Azelio model, with a maximum difference nearing +1.8 kW. These results are considered acceptable, considering the significant differences in the modelling approach. Therefore, the proposed linearized model model is considered valid for the performed studies.

Finally, the comparison of the proposed linearized model and Azelio TES.POD models in terms of residual heat is shown in Fig. 16. As the residual heat profile is directly linked to the one of the power outputs, the conclusions drawn regarding the latter apply in this case as well. It is interesting to discuss about how the Stirling engine efficiency comes into effect. The thermal power difference spikes between the 10<sup>th</sup> and 12<sup>th</sup> hour in Fig. 16 can be explained by a change in Stirling engine setpoint in the Azelio TES.POD model leading to higher efficiency (and therefore less residual heat) compared to the proposed linearized model. Similarly, it is interesting to notice that that the thermal power output difference decreases while the power output difference increases by the end of the second discharge in Fig. 16. This happens because of the temperature tapering in the Azelio model, causing the efficiency of the Stirling engine to decrease and the amount of heat that the cooling system needs

to cool to increase. On average, the proposed linearized model supplied +1.09 kW thermal additional power compared to the Azelio model.

## VI. CONCLUSION

This paper presented an IGDT based EMS for optimal heat and power scheduling in LECs. A novel enthalpy-temperature based model for the TES was specifically designed for application in MILPs and validated by real time studies of Azelio industrial TES. The validation study revealed that the proposed model exhibits a high level of accuracy when compared to the real-time model. This suggests that the model reliably captures the behavior and performance of the TES system while it can effectively be used in both operational and planning MILP studies. The role of Azelio TES.POD on enhancing the PV hosting capacity of the LEC was investigated and shown that hosting capacity can be increase to more than 75% without any PV curtailment. The uncertainties of PV and load were modeled by IGDT method, and the Pareto front optimal solutions showed with increasing the UB more robustness is provided against forecast errors of PV and load. The best solution among Pareto optimal front was selected based on the accuracy of the conducted forecasts and the results were presented. A Monte-Carlo simulation was conducted with considering the PDFs of forecasted errors of load demand and PV power retrieved from the forecasts. It was shown that with selecting the appropriate UB, the prespecified operation cost can be guaranteed. Compared with SO and RO, the IGDT-based model is notably more robust, albeit with slightly higher costs than SO. The suggested future direction involves conducting a practical EMS to co-optimize energy and flexibility utilizing Azelio thermal energy storage within the LEC.

## REFERENCES

- [1] S.-L. Penttinen, P. Aalto, and T. Haukkala, *EU Electricity Market Reform and the Adoption of the Clean Energy Package Addressing System Flexibility*. Bandung, Indonesia: Eltran, 2020.
- [2] S. Kuravi, J. Trahan, D. Y. Goswami, M. M. Rahman, and E. K. Stefanakos, "Thermal energy storage technologies and systems for concentrating solar power plants," *Prog. Energy Combustion Sci.*, vol. 39, no. 4, pp. 285–319, 2013.
- [3] S. Wong and J.-P. Pinard, "Opportunities for smart electric thermal storage on electric grids with renewable energy," *IEEE Trans. Smart Grid*, vol. 8, no. 2, pp. 1014–1022, Mar. 2016.
- [4] J. Kiviluoma et al., "Harnessing flexibility from hot and cold: Heat storage and hybrid systems can play a major role," *IEEE Power Energy Mag.*, vol. 15, no. 1, pp. 25–33, Jan./Feb. 2017.
- [5] M. Jadidbonab, B. Mohammadi-Ivatloo, M. Marzband, and P. Siano, "Short-term self-scheduling of virtual energy hub plant within thermal energy market," *IEEE Trans. Ind. Electron.*, vol. 68, no. 4, pp. 3124–3136, Apr. 2020.
- [6] M. M. Bidgoli, H. Karimi, S. Jadid, and A. Anvari-Moghaddam, "Stochastic electrical and thermal energy management of energy hubs integrated with demand response programs and renewable energy: A prioritized multi-objective framework," *Electric Power Syst. Res.*, vol. 196, 2021, Art. no. 107183.
- [7] D. Steen, M. Stadler, G. Cardoso, M. Groissböck, N. DeForest, and C. Marnay, "Modeling of thermal storage systems in MILP distributed energy resource models," *Appl. Energy*, vol. 137, pp. 782–792, 2015.
- [8] G. Tk and V. Raj, "Use of phase change material (PCM) for the improvement of thermal performance of cold storage," *MOJ Curr. Res. Rev.*, vol. 1, no. 2, pp. 49–61, 2018.

- [9] Y. Dai et al., "A general model for thermal energy storage in combined heat and power dispatch considering heat transfer constraints," *IEEE Trans. Sustain. Energy*, vol. 9, no. 4, pp. 1518–1528, Oct. 2018.
- [10] Y. Dai et al., "Integrated dispatch model for combined heat and power plant with phase-change thermal energy storage considering heat transfer process," *IEEE Trans. Sustain. Energy*, vol. 9, no. 3, pp. 1234–1243, Apr. 2017.
- [11] F. Wei et al., "A novel thermal energy storage system in smart building based on phase change material," *IEEE Trans. Smart Grid*, vol. 10, no. 3, pp. 2846–2857, May 2018.
- [12] Q. Chen, "Entransy dissipation-based thermal resistance method for heat exchanger performance design and optimization," *Int. J. Heat Mass Transfer*, vol. 60, pp. 156–162, 2013.
- [13] M. Mohiti, M. Mazidi, N. Rezaei, and M. - H. Khooban, "Role of vanadium redox flow batteries in the energy management system of isolated microgrids," *J. Energy Storage*, vol. 40, 2021, Art. no. 102673.
- [14] M. Kermani, E. Shirdare, A. Najafi, B. Adelmanesh, D. L. Carni, and L. Martirano, "Optimal self-scheduling of a real energy hub considering local DG units and demand response under uncertainties," *IEEE Trans. Ind. Appl.*, vol. 57, no. 4, pp. 3396–3405, Oct. 2021.
- [15] Y. Li, M. Han, M. Shahidehpour, J. Li, and C. Long, "Data-driven distributionally robust scheduling of community integrated energy systems with uncertain renewable generations considering integrated demand response," *Appl. Energy*, vol. 335, 2023, Art. no. 120749.
- [16] M. Tostado-Véliz, A. R. Jordehi, S. A. Mansouri, and F. Jurado, "A two-stage IGDT-stochastic model for optimal scheduling of energy communities with intelligent parking lots," *Energy*, vol. 263, 2023, Art. no. 126018.
- [17] M. Dolanyi, K. Bruninx, J. - F. Toubeau, and E. Delarue, "Risk-based constraints for the optimal operation of an energy community," *IEEE Trans. Smart Grid*, vol. 13, no. 6, pp. 4551–4561, Jun. 2022.
- [18] M. Jasinski et al., "Operation and planning of energy hubs under uncertainty—a review of mathematical optimization approaches," *IEEE Access*, vol. 11, pp. 7208–7228, 2023.
- [19] S. Dorahaki, M. Rashidinejad, S. F. F. Ardestani, A. Abdollahi, and M. R. Salehizadeh, "Probabilistic/information gap decision theory-based bilevel optimal management for multi-carrier network by aggregating energy communities," *IET Renewable Power Gener.*, vol. 17, no. 6, pp. 1436–1465, 2023.
- [20] D. Masihabadi, M. Kalantar, Z. Majd, and S. V. S. Saravi, "A novel information gap decision theory-based demand response scheduling for a smart residential community considering deep uncertainties," *IET Gener., Transmiss. Distrib.*, vol. 17, no. 6, pp. 1383–1399, 2023.
- [21] "Azelio thermal energy storage." Accessed: Feb. 8, 2024. [Online]. Available: <https://www.azelio.com/the-solution/technology/>
- [22] "Modular control systems for maximizing solar energy utilization and grid service provisions by residential PV systems coupled with thermal storage." [Online]. Available: <https://sunsets.upatras.gr/>
- [23] M. Mohiti, M. Mazidi, and D. Steen, "A risk-averse energy management system for optimal heat and power scheduling in local energy communities," in *Proc. IEEE Int. Conf. Environ. Elect. Eng. IEEE Ind. Commercial Power Syst. Europe*, 2022, pp. 1–6.
- [24] M. Yazdanejad, N. Amjadi, and S. Dehghan, "VPP self-scheduling strategy using multi-horizon IGDT, enhanced normalized normal constraint, and bi-directional decision-making approach," *IEEE Trans. Smart Grid*, vol. 11, no. 4, pp. 3632–3645, Jul. 2019.
- [25] M. Mazidi, H. Monsef, and P. Siano, "Robust day-ahead scheduling of smart distribution networks considering demand response programs," *Appl. Energy*, vol. 178, pp. 929–942, 2016.



**Maryam Mohiti** received the B.Sc. and M.Sc. degrees from the Sharif University of Technology, Tehran, Iran, in 2011 and 2013, respectively, and the Ph.D. degree in electrical engineering from the University of Tehran, Tehran, Iran, 2019. She is currently a postdoc Researcher with the Chalmers University of Technology, Gothenburg, Sweden. Her research interests include microgrids, energy storages, energy systems, and energy forecast.



**Mohammadreza Mazidi** received the B.S. and M.S. degrees in electrical engineering from the Iran University of Science and Technology, Tehran, Iran, in 2010 and 2012, respectively, and the Ph.D. degree from the University of Tehran, Tehran, in 2016. He is currently a Researcher with the Chalmers University of Technology, Gothenburg, Sweden. His research interests include renewable-based power system planning, operation, and control and energy systems.



**Niccolò Oggioni** received the B.Sc. degree in energy engineering from the Alma Mater Studiorum University of Bologna, Italy, in 2017, and the M.Sc. degree in sustainable energy engineering from the Royal Institute of Technology, Stockholm, Sweden, in 2019. Between 2019 and 2023, he was part of the Research and Technology team as a System Engineer with Azelio AB, where he developed models of thermal energy storage based on phase-change materials. He is currently a Energy Storage Product Specialist with Soltech Energy Solutions, where he supports and

optimizes the operation and maintenance of BESS power plants in Sweden.



**David Steen** received the M.Sc. and Ph.D. degrees in electrical engineering from the Chalmers University of Technology, Gothenburg, Sweden, in 2008 and 2014, respectively. He is currently a Researcher with the Department of Electrical Engineering, Chalmers University of Technology. His research interests include modeling and control of integrated energy systems and distributed energy resources such as solar PV, wind power, electric vehicles, and energy storage.



**Le Anh Tuan** (Member, IEEE) received the B.Sc. degree in power systems from the Hanoi University of Technology, Hanoi, Vietnam, in 1995, the M.Sc. degree in energy economics from the Asian Institute of Technology, Bangkok, Thailand, in 1997, and the Ph.D. degree in power systems from the Chalmers University of Technology, Gothenburg, Sweden, in 2004. He is currently an Associate Professor with the Division of Electric Power Engineering, Department of Electrical Engineering, Chalmers University of Technology. His research interests include modeling,

optimization, control and protection of integrated energy systems, and active distribution networks with high level of renewables and energy storage, wide-area monitoring and control of large power transmission systems, machine learning applications to power systems, modeling and design of energy, and ancillary service markets.